CRYSTAL GROWTH & DESIGN

Article

pubs.acs.org/crystal

Single Crystals of C12A7 ($Ca_{12}Al_{14}O_{33}$) Substituted with 1 mol % Iron

Stefan G. Ebbinghaus,*[,†] Holger Krause,[†] Doh-Kwon Lee,*[,‡] and Jürgen Janek[§]

[†]Martin-Luther-Universität Halle-Wittenberg, Institut für Chemie, Kurt-Mothes-Straße 2, D-06120 Halle/Saale, Germany

[‡]Photo-electronic Hybrids Research Center, Korea Institute of Science and Technology (KIST), Seoul 136-791, Korea

[§]Justus-Liebig-Universität Gießen, Institut für Physikalische Chemie, Heinrich-Buff-Ring 58, D-35392 Gießen, Germany

ABSTRACT: Single crystals of $Ca_{12}Al_{14}O_{33}$ (C12A7, mayenite) substituted with 1 mol % Fe were grown by the floating zone technique in an atmosphere of 2% O_2/98% N_2. The iron substitution leads to an increase of the unit cell parameter by roughly 0.002 Å. Optical spectroscopy reveals an additional broad absorption band at 310 nm for the iron-substituted sample reflecting the yellow color of the crystals. XANES measurements at the Fe−K absorption edge prove the incorporation of Fe^{3+} on the aluminum sites. Measurements of the magnetic susceptibility resulted in a value of 5.8 μ_B per iron ion as expected for high-spin Fe^{3+}. C12A7 is known to be a very good oxygen ion conductor at high temperatures. In pure oxygen, the iron substitution leads to a slightly reduced conductivity between approximately 500 and 800 °C, while at higher temperatures, the conductivity is very similar to the pristine material. Under reducing conditions, the slope of $\log(\sigma)$ vs $\log(p(O_2))$ of the iron-substituted sample was found to be steeper than that for pure C12A7.

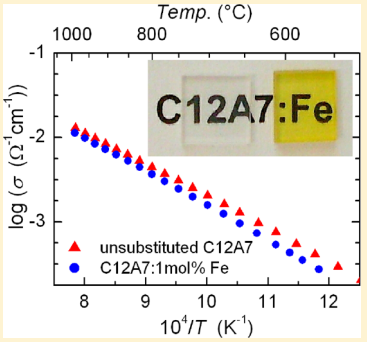

INTRODUCTION

$Ca_{12}Al_{14}O_{33}$ is a very good oxygen ion conductor at high temperatures with a conductivity only about 1 order of magnitude below that of yttria-stabilized zirconia (YSZ).[1−3] $Ca_{12}Al_{14}O_{33}$ naturally occurs as the mineral mayenite and is known to be a component of special types of concrete, where it is often denoted as C12A7 due to its formal composition $12CaO{\cdot}7Al_2O_3$. The exceptional properties of mayenite result from its cage-like crystal structure, which can be described as a positively charged $(C_{12}Al_{14}O_{32})^{2+}$ framework, in which 1/6 of the cages are occupied by oxygen ions. The high ionic conductivity makes mayenite an interesting material for various applications including solid oxide fuel cells, oxygen gas sensors, or oxidation catalysis. In addition, the cage oxygen ions can be replaced by F^-, Cl^-, or OH^-[4,5] and even "exotic" ions like O^-, O_2^-, H^-, and e^-.[6−8] As shown recently, nitrogen-containing species can also be incorporated.[9,10]

While pure and anion-substituted C12A7 phases have been intensively studied, comparatively little is known about the effect of cation substitutions on the aluminum site.

Cosubstitution with Zn and P leading to $Ca_{12}Al_{14-x-y}Zn_xP_yO_z$ with $z = 33 + y - x/2$, $0 < x < 0.66$ and $0 < y < 0.33$ was reported in ref 11 and was found to slightly decrease the ionic conductivity.

Si-containing mayenite with the composition $Ca_{12}Al_{10}Si_4O_{35}$ was synthesized by heating the hydrogarnet $Ca_3Al_2(SiO_4)_{0.8}(OH)_{8.8}$ at 800 °C for 15 h.[12] The higher charge of silicon compared with aluminum results in an enhanced oxygen content. The sample was found to catalyze the decomposition of various hydrocarbons and fix HCl gas at high temperatures. By the same approach, samples with varying silicon content $Ca_{12}Al_{(14-x)}Si_xO_{(33+x/2)}$ (x = 2, 3, or 4) can also be obtained.[13] After hydrogen ion implantation and UV irradiation, the compounds exhibited an electronic conductivity that increases with x. A small polaron transport mechanism was proposed. It is noteworthy that Si-containing mayenite is not thermally stable but starts to decompose at 600 °C.[13]

EPR measurements were performed on copper-doped C12A7 and three different Cu^{2+} species were identified.[14] In ref 9, powder neutron diffraction of C12A7 doped with 0.1% and 2.5% Fe was reported. The higher iron content was found to reduce the incorporation of hydrogen in the cage framework. Finally, Czochralski crystal growth in Ir crucibles leads to $Ca_{12}Al_{14}O_{33}$ with small amounts of Ir^{4+} incorporated.[15] To the best of our knowledge, these Ir-doped crystals are the only example of C12A7 single crystals containing a transition metal.

In this paper, we report on single crystals of mayenite substituted with 1 mol % iron ($Ca_{12}Al_{13.86}Fe_{0.14}O_{33}$). The incorporation of a transition metal is interesting because the physical properties, especially the oxygen ion conductivity, may be altered. Since hydroxyl groups within the cages reduce the conductivity[16] and iron substitution reduces the amount of hydrogen,[9] the presence of Fe might lead to an enhanced ion conductivity. Furthermore, iron is a redox active element, so by thermal treatment in oxidizing or reducing atmospheres, the amount of cage oxide ions might be tailored via the reduction to Fe^{2+} or (partial) oxidation to Fe^{4+}. Again, this may result in modified electrical conductivities. Iron can also act as a local probe to investigate the incorporation and release of oxygen from the framework, for example, by optical spectroscopy. Finally, the high spin state of Fe^{3+} (S = 5/2) makes this ion interesting for investigations of the local structure by EPR. Such

Received: December 6, 2013
Revised: February 18, 2014
Published: February 21, 2014

   dx.doi.org/10.1021/cg401823k | *Cryst. Growth Des.* 2014, 14, 2240−2245

investigation can help to identify the binding mode of the cage oxygen and its transport mechanism.

EXPERIMENTAL SECTION

Single-phase polycrystalline $Ca_{12}Al_{13.86}Fe_{0.14}O_{33}$ was prepared by solid-state synthesis from α-Al_2O_3 (99.999%, Pengda), Fe_2O_3 (99.99%, ChemPur) and $CaCO_3$ (pro analysis, Merck). An excess of 1 mol % Al_2O_3 was used to avoid the formation of $Ca_3Al_2O_6$ (C3A). Appropriate amounts of the starting agents were wet ground with isopropanol for 12 h in a planetary ball mill (Fritsch Pulverisette 5.202). The obtained powder mixture was heated in covered alumina crucibles for 24 h at 1250 °C in a box furnace in air (heating and cooling rates 300 °C/h). Phase purity of the product was checked by powder X-ray diffraction, and no secondary phases were detected.

The floating zone growth of single crystals was performed in a Crystal Systems Corporation optical floating zone furnace model FZ-T-10000-H-VPO-PC equipped with four 1500 W halogen lamps. Details of the growth procedure are described in ref 17. In short, a two-step procedure was applied in which the polycrystalline sintered rod of C12A7:Fe was first molten with 5 mm/h in an atmosphere consisting of 2% O_2/98% N_2. In a second crystallization run, a much slower growth rate of only 0.2 mm/h was applied. By this procedure, clear and defect free crystals of roughly 1 cm width with length of several centimeters were obtained. These crystals were cut into slices using a diamond wheel saw and polished with 1 μm diamond dispersion for the optical investigations.

A small piece of the crystal (ca. 100 mg) was crushed and dissolved in hydrochloric acid. The iron content was measured spectroscopically using the Merck Spectroquant iron test kit (reduction to Fe^{2+} and formation of a red-violet complex in thioglycolate-buffered solution). The obtained value of 5.56(5) mg of iron per gram of sample corresponds to 0.99(1) mol % Fe, which is very close to the nominal value.

UV−vis measurements were carried out in transmission mode with 2 nm resolution, a spot size of 100 × 100 μm^2 and an integration time of 0.3 s with a Zeiss MPM 800 microscope spectral photometer.

X-ray absorption spectroscopy at the Fe−K edge was performed at the beamline A1 of the Hamburger Synchrotronstrahlungslabor (HASYLAB) at Deutsches Elektronensynchrotron (DESY). A small amount of powder from a piece of crushed crystal was stuck to adhesive tape, which was folded several times to obtain a reasonable edge jump while keeping the absorption relatively low. XANES measurements were performed in transmission mode with a step width of 0.2 eV and a counting time of 2 s per data point. To increase the signal-to-noise ratio, measurements were repeated four times and averaged. The incident X-ray beam was energy-resolved using a Si(111) double crystal monochromator. Higher-order harmonic contributions were suppressed by detuning the second monochromator crystal to 50% of the maximum intensity. The energy was calibrated against the first inflection point of an Fe metal foil, which was measured simultaneously. The obtained XANES spectra were processed using the program *WinXAS*.[18] The background correction was performed by a linear fit in the energy range 7.070−7.100 keV, and the spectra were normalized to the maximum of the absorption.

Magnetic measurements were carried out using a Quantum Design PPMS-9 system. The samples were enclosed in gel capsules whose small contribution to the magnetic susceptibility was taken into account by a temperature-independent parameter, χ_0, in the data-fitting procedure. Measurements were performed both under zero-field-cooled (zfc) and field-cooled (fc) conditions in external magnetic fields of 20 and 50 kOe. The diamagnetic contribution of the core electrons was accounted for by subtracting the (temperature-independent) susceptibility of pure $Ca_{12}Al_{14}O_{33}$.

For conductivity measurements, a crystal slice was cut into a parallelepiped of 1.7 × 1.6 × 7 mm^3. The surface was polished down to 1 μm grit. Conductivity was measured by dc four-probe method (Keithley 2700, 224) as a function of temperature in the range of 570 °C < T < 1000 °C in dry oxygen atmosphere. The gas was dehumidified with the aid of P_2O_5 and molecular sieve F1510634 (Merck). Additional measurements were performed as a function of the oxygen partial pressure, $p(O_2)$, in the range of $-19 < \log[p(O_2)/\text{bar}] < 0$ in dry conditions at 800, 900, and 1000 °C, respectively. The oxygen activity in the atmosphere was controlled using CO_2/CO and Ar/O_2 gas mixtures and was monitored with a zirconia-based oxygen sensor that was kept at the same temperature as the sample within ±2 °C.

RESULTS AND DISCUSSION

The crystal growth of iron-substituted mayenite yielded yellow colored boules, while pure mayenite is completely colorless as shown in Figure 1. It is worth noting that the intensity of

Figure 1. Photograph of polished single-crystalline slices (ca. 5 mm × 5 mm) of pure C12A7 (left) and C12A7 substituted with 1 mol % iron (right).

coloring did not change along the growth direction indicating a homogeneous iron distribution. From the obtained crystal ingots several small cubes (0.2 mm × 0.2 mm × 0.2 mm) were cut and investigated by single crystal X-ray diffraction. All cubes were found to be single crystalline. Since the results of the structural analysis were nearly identical to the ones listed in the Supporting Information of a preceding paper,[17] they are not explicitly given here.

Powder X-ray diffraction carried out on crushed pieces of the crystals revealed complete phase purity. The cubic cell parameter was determined as a = 11.9904(4) Å, which is only 0.17‰ larger compared with the unsubstituted material (11.9883(3) Å). Such small differences are not surprising taking into account the low substitution level and the similar ionic radii of Fe^{3+} and Al^{3+} in tetrahedral oxygen coordination (0.49 and 0.39 Å, respectively[19]). It is to be noted, though, that the differences between the pure and iron-substituted samples are indeed significant and identical values (within the given error range) were obtained for various batches.

The color change due to iron substitution is reflected by the UV−vis spectra depicted in Figure 2. To obtain reasonable absorptions, a crystal with a lower iron content of 0.5 mol % was used. Spectra recorded at different positions of a crystal slice with approximately 90 μm thickness were found to be identical. The incorporation of iron results in a broad absorption band with a maximum at approximately 310 nm (4.0 eV) as best seen by subtracting the absorption of pure mayenite. Additional investigations using a PerkinElmer Lambda 900 spectrometer showed that no other features occur up to 3300 nm, i.e., in the infrared region, where the absorption bands of tetrahedrally coordinated Fe^{2+} are located.[20] As will be shown in the following, iron occupies the aluminum sites of the C12A7 framework and possesses the oxidation state +3. On both possible Al sites of the crystal structure, iron has a rather regular tetrahedral oxygen coordination resulting in a $(e)^2(t_2)^3$ electronic configuration

dx.doi.org/10.1021/cg401823k | *Cryst. Growth Des.* 2014, 14, 2240−2245

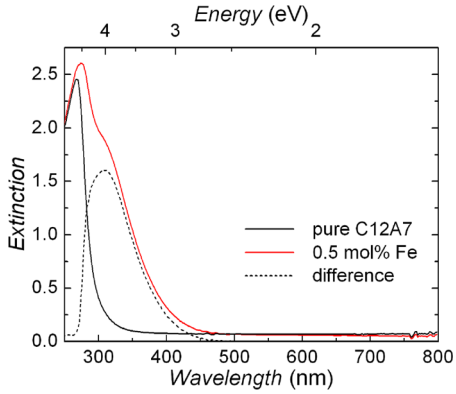

Figure 2. UV−vis spectra of pure and Fe-substituted C12A7.

corresponding to the ground term $^6A_1$. From molecular orbital calculations of tetrahedral $(FeO_4)^{5-}$ clusters, Sherman determined the energies of possible transitions.[21] Using the values given in this reference, the absorption maximum at 310 nm can be assigned to the (spin-forbidden) transition from the $^6A_1$ ground term to the $^4T_2$ state arising from the ^4D term of the free ion. The optical spectra of C12A7:Fe can additionally be compared with the one of iron-doped γ-$LiAlO_2$, in which Fe^{3+} substitutes for aluminum in tetrahedral coordination, too.[22] The absorption band of iron in mayenite roughly agrees with the value of ∼390 nm found for γ-$LiAlO_2$:Fe. On the other hand, a second peak at ∼450 nm in this compound is clearly missing for C12A7:Fe (Figure 2), resulting in visibly different colors: iron-doped γ-$LiAlO_2$ was reported to have a yellow green color, while C12A7:Fe is pure yellow as seen in Figure 1. The difference in the optical spectra may result from a much lower iron content of 0.5 mol % compared with 6 mol % in γ-$LiAlO_2$:Fe. Higher iron contents can lead to more intense absorptions due to magnetic interactions of neighboring iron sites, which preserve the (total) spin state during the electronic transition.[21]

To prove the incorporation of iron in the mayenite framework and to determine its oxidation state, X-ray absorption spectroscopy was used. Due to the low iron content of only 1%, it was not possible to carry out EXAFS investigations. On the other hand, important conclusions can already be drawn from the near-edge region (XANES), which provides information on the oxidation state and the local environment of the absorbing element. Especially the pre-edge features are known to be very sensitive to the symmetry of the coordination sphere. In a surrounding with inversion symmetry like the octahedral coordination, the pre-edge peaks are very small, while in coordination geometries without an inversion center (e.g., tetrahedral coordination), the pre-edge features are by far more pronounced. The peak intensity of the 1s → 3d transition can therefore serve to directly distinguish between different coordination geometries. In addition, the exact energy position of the pre-edge peaks is a highly reliable measure for the oxidation state of the absorbing element. With increasing oxidation number, the peaks are shifted toward higher energies. The origin for this so-called valence shift lies in the partial shielding of the atomic core charge by the valence electrons. When the oxidation state increases, the number of valence electrons is reduced and the effective core charge in turn increases, leading to tighter binding of the electrons. Therefore, the energy required to promote an electron to a vacant bound state (or for photoionization) increases, which results in a corresponding shift of the absorption edge. The effect is in the range of 1−2 eV per oxidation number and can well be measured. In earlier investigations, we have used the valence shift to determine the oxidation state of various transition metals.[23−27]

In Figure 3, the pre-edge region of the Fe−K XANES spectrum of a powder from a crushed C12A7:Fe crystal is

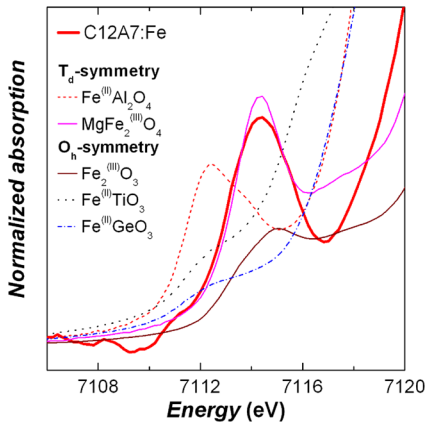

Figure 3. Fe−K XANES of iron substituted C12A7 in comparison to references containing Fe^{2+} or Fe^{3+} in tetrahedral and octahedral oxygen coordination geometry.

depicted. For comparison, we measured various reference oxides in which iron occupies tetrahedral sites ($FeAl_2O_4$ and $MgFe_2O_4$) or octahedral sites (Fe_2O_3, $FeTiO_3$, and $FeGeO_3$). In $FeAl_2O_4$, $FeTiO_3$, and $FeGeO_3$ iron shows the oxidation state 2+, while in $MgFe_2O_4$ and Fe_2O_3 iron is in the oxidation state 3+.

From Figure 3, it is evident that the energy position of the observed pre-edge peak is in excellent accordance with the ones of the Fe^{3+} references. This proves that the iron ions incorporated in the mayenite framework take the oxidation state 3+. In addition, the intensity of the pre-edge peak, as well as its shape, corresponds very well to iron in tetrahedral oxygen coordination. This can best be seen comparing the XANES of C12A7:Fe with the one of the inverse spinel $MgFe_2O_4$. The pre-edge structures of both compounds are basically identical indicating a tetrahedral oxygen coordination for iron.

This interpretation is further supported by comparison of our findings with earlier investigations by Wilke et al. In ref 28, the pre-edge features of numerous iron oxides were studied in detail. As one of the main results, it was found that the pre-edge structure of Fe^{3+} in T_d geometry can be described by a single peak positioned at approximately 7114 eV, while the structure of the pre-edge is by far more complex (consisting of at least two overlapping peaks) for O_h symmetry. For Fe^{2+}, complex, pre-edge features (two or three peaks) are observed for both T_d and O_h symmetry, and the centroid of the peaks is shifted to a lower energy of approximately 7112 eV. Comparing these values with the spectra depicted in Figure 3 reveals that our spectra for iron-substituted C12A7 correspond to Fe^{3+} in T_d geometry as expected for iron incorporated on the Al sites of $Ca_{12}Al_{14}O_{33}$.

Magnetic measurements were carried out for different external fields, as shown in Figure 4. For clarity, the molar susceptibility, χ_{mol} (left scale), is given for the 20 kOe measurement only. As seen from the reciprocal susceptibilities (right scale), the results are independent of the magnetic field.

dx.doi.org/10.1021/cg401823k | Cryst. Growth Des. 2014, 14, 2240−2245

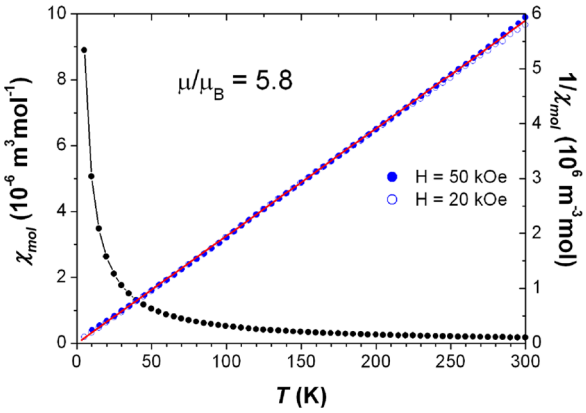

Figure 4. Magnetic susceptibility per mole iron of C12A7 containing 1 mol % Fe. The right scale shows the inverse susceptibility for two different fields (circles) and the fit (solid red line) by a modified Curie–Weiss law.

No deviations between zfc and fc data were observed, either. The susceptibility clearly follows a Curie–Weiss behavior as expected for diluted iron ions. Pure mayenite was found to have a temperature-independent diamagnetic molar susceptibility of $-0.0162(6) \times 10^{-6}$ m^3 mol^{-1}. Measurements of the iron-containing samples were corrected for this value prior to data analysis. In addition, a small temperature-independent term was included in the fit procedure to take into account varying contributions of the sample carrier. For data evaluation, the reciprocal molar susceptibilities were fitted by a modified Curie–Weiss law, $\chi_{mol} = C/(T - \theta) + \chi_0$. For θ, very small values between -2 and -0.5 K were found indicating noninteracting magnetic centers as expected.

Assuming an iron content of 1 mol %, the obtained magnetic moment per Fe ion of 5.8(1) μ_B corresponds very well with the value of 5.916 μ_B expected for Fe^{3+} in high-spin configuration. This finding is in accordance with iron substituting Al, since in a tetrahedral coordination Fe^{3+} is in the high-spin state ($e^2t_2^3$). In addition, the good agreement between expected and experimentally found magnetic moments indicates that the amount of incorporated iron is very close to the nominal value of 1 mol %.

The electrical conductivity of iron substituted C12A7 was found to be similar to the undoped material.[3] In Figure 5, the conductivity in dry oxygen is shown as a function of temperature in an Arrhenius plot. The applied measurement conditions did not alter the sample as evidenced by identical values during heating and cooling (solid and open symbols).

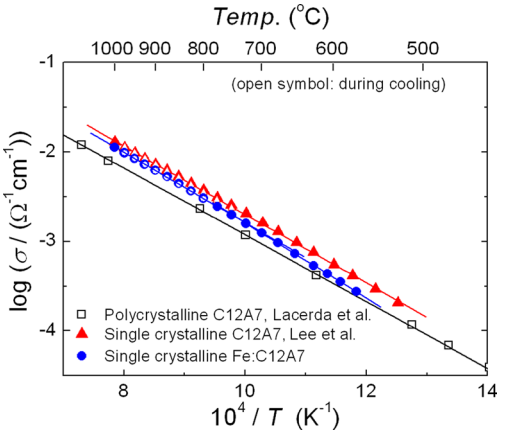

Figure 5. Arrhenius plot of the total electrical conductivity, σ, vs temperature for single crystalline C12A7 substituted with 1 mol % Fe in comparison to single crystalline[3] and polycrystalline[1] pure material.

As can be seen from Figure 5, the conductivity of Fe-substituted C12A7 is slightly smaller than that of the undoped material, especially at lower temperatures. With increasing temperature, the differences become smaller, as reflected by a slightly steeper slope for C12A7:Fe. A closer inspection reveals a minor change in the slope leading to activation energies of 0.780(3) eV in the range above 725 °C, while for lower temperatures an even higher value of 0.835(3) eV was found. These values are slightly larger than the one of 0.758(4) eV recently found for the undoped single crystalline material.[3] Although the difference in activation energy is comparatively small, it indicates a clear effect even of small iron contents.

Figure 6 represents the conductivity as a function of oxygen partial pressure at 800, 900, and 1000 °C. In the high oxygen

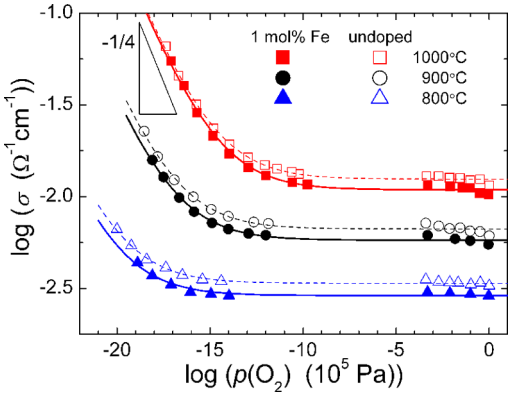

Figure 6. Double logarithmic plot of the total electrical conductivity of 1 mol % Fe-substituted and pure $Ca_{12}Al_{14}O_{33}$ as a function of the oxygen activity. The solid and dashed curves are fits to the equation, $\sigma = \sigma_n^\circ p(O_2)^{-1/4} + \sigma_O$.

partial pressure regime (10^5–10^2 Pa), for both the pure and the 1 mol % Fe substituted C12A7, almost constant values were found. This plateau can be assigned to the ionic conductivity from the mobile cage oxygen ions.[3] Since both Al^{3+} and Fe^{3+} possess the same charge, the iron substitution is not expected to significantly alter the concentration of cage oxygen ions. Thus, the reduced conductivity can be explained by a lower mobility of these oxide ions, reflecting a tighter binding to iron in comparison to aluminum.

As already observed in the temperature-dependent measurements, the conductivity differences between the pure and the Fe-substituted mayenite become smaller as the temperature increases. At very low oxygen activities, that is, below 10^{-5} Pa, the conductivity strongly increases with decreasing $p(O_2)$. For both the pure and the iron-substituted material, the conductivity isotherms can be well fitted by $\sigma = \sigma_n^\circ p(O_2)^{-1/4} + \sigma_O$, where σ_n° and σ_O denote the electronic partial conductivity at $p(O_2) = 1$ bar and the ionic conductivity, respectively. Corresponding values are listed in Table 1. Interestingly, for the iron substituted material, the slope below roughly 10^{-10} Pa is slightly steeper. This effect becomes more pronounced at higher temperatures, and at 1000 °C, the total conductivity of C12A7:Fe reaches the same values as the unsubstituted material. As has been pointed out in ref 3, the relation $\sigma \propto p(O_2)^{-1/4}$ is valid if the concentration of cage

dx.doi.org/10.1021/cg401823k | Cryst. Growth Des. 2014, 14, 2240–2245

Table 1. Fit Values for σ_n° and σ_O for Pure and Iron-Substituted C12A7 Derived from the Conductivity Isotherms in Figure 6

	$\log(\sigma_n^\circ/\Omega^{-1}\cdot cm^{-1})$		$\log(\sigma_O/\Omega^{-1}\cdot cm^{-1})$	
temp, °C	C12A7	C12A7:Fe	C12A7	C12A7:Fe
800	−7.50(12)	−7.60(4)	−2.472(3)	−2.539(6)
900	−6.45(2)	−6.54(2)	−2.176(5)	−2.237(5)
1000	−5.64(1)	−5.66(1)	−1.905(4)	−1.963(6)

oxygen is comparable to that of the positively charged cages, that is, if the material is basically the oxygen mayenite $[Ca_{12}Al_{14}O_{32}]:O^{2-}$. The steeper slope observed for the iron-substituted C12A7 at very low oxygen activities, which is still below 0.25, indicates that the transition between the predominant conduction regimes (from plateau ionic conductivity to the electronic one with $\sigma \propto p(O_2)^{-1/4}$) takes place at higher $p(O_2)$ for the Fe-substituted sample. This implies that iron substitution shifts the beginning of electride formation toward higher oxygen activities. Further experiments on samples with larger iron contents or at lower oxygen activities are planned for the future to verify this assumption.

CONCLUSIONS

This paper reports on the first investigations of single-crystalline $Ca_{12}Al_{14}O_{33}$ substituted with significant amounts (i.e., well above the doping level) of iron. Single crystals of mayenite (C12A7) containing 1 mol % iron were successfully grown by the floating zone technique. The uniform yellow coloring of the crystals indicates a homogeneous iron distribution. Optical spectroscopy shows a broad absorption band with a maximum at 310 nm that can be assigned to the transition from the $^6A_1$ ground state to the $^4T_2$ state arising from the free-ion ^4D term. Possible inclusions of submicroscopic iron oxide particles can be ruled out for C12A7:Fe since the substitution leads to a small yet significant and reproducible increase of the unit cell parameter by approximately 0.002 Å, reflecting the larger ionic radius of Fe^{3+} compared with Al^{3+}. More important, X-ray absorption spectroscopy at the Fe−K edge unambiguously revealed a tetrahedral oxygen coordination of iron in accordance with Fe occupying Al sites in the mayenite framework. Additionally, from the valence shift, an oxidation state of +3 was found for iron. This finding is further supported by magnetic measurements yielding 5.8 μ_B per iron ion in agreement with the expected spin-only value for high-spin Fe^{3+}. The good agreement between expected and measured magnetic moment as well as a quantitative Fe analysis furthermore prove that the iron content is close to the nominal value of 1 mol %.

Electrical conductivity measurements in oxygen showed that the iron substitution leads to slight reduction of the oxide ion mobility, which dominates the charge transport. This can be assigned to a tighter binding of the cage oxide ions to iron. On the other hand, at 1000 °C, the conductivities of the iron-substituted and the pure mayenite become very similar due to the higher activation energy found for C12A7:Fe. Under reducing conditions ($p(O_2) < 10^{-10}$ Pa), a steeper slope than for pure mayenite was observed, indicating that the beginning of electride formation is shifted toward higher oxygen activity.

Because of the low substitution level of 1 mol %, it is not surprising that the effects are small. Additional investigations on samples with higher substitution levels would be highly desirable. Unfortunately, our attempts to grow such single crystals have not been successful until now, but further trials are planned for the future.

AUTHOR INFORMATION

Corresponding Authors

*Prof. Dr. Stefan G. Ebbinghaus. Phone: +49-(0)345-55-25870. Fax: +49-(0)345-55-27028. E-Mail: stefan.ebbinghaus@chemie.uni-halle.de.

*Dr. Doh-Kwon Lee. Phone: +82-(0)2-958-6710. Fax: +82-(0)2-958-6649. E-mail: dklee@kist.re.kr.

Notes

The authors declare no competing financial interest.

ACKNOWLEDGMENTS

Financial support by the Deutsche Forschungsgemeinschaft (DFG) through Grants EB 219/4-1 and JA 648/20-1 is highly acknowledged. The optical floating zone furnace was supported by the DFG through Grant INST 271/258-1 FUGG. The authors are gratefully to Christine Seidel for help with the optical spectroscopy. Further thanks are due to HASYLAB for allocating beamtime and to Dr. Edmund Welter for technical assistance.

REFERENCES

(1) Lacerda, M.; Irvine, J. T. S.; Glasser, F. P.; West, A. R. *Nature* **1988**, *332*, 525−526.

(2) Irvine, J. T. S.; Lacerda, M.; West, A. R. *Mater. Res. Bull.* **1988**, *23* (7), 1033−1038.

(3) Lee, D.-K.; Kogel, L.; Ebbinghaus, S. G.; Valov, I.; Wiemhöfer, H.-D.; Lerch, M.; Janek, J. *Phys. Chem. Chem. Phys.* **2009**, *11*, 3105−3114.

(4) Jeevaratnam, J.; Glasser, F. P.; Dent Glasser, L. S. *J. Am. Ceram. Soc.* **1964**, *47* (2), 105−106.

(5) Hayashi, K.; Hirano, M.; Hosono, H. *J. Phys. Chem. B* **2005**, *109* (24), 11900−11906.

(6) Hayashi, K.; Hirano, M.; Matsuishi, S.; Hosono, H. *J. Am. Chem. Soc.* **2002**, *124* (5), 738−739.

(7) Hayashi, K.; Matsuishi, S.; Kamiya, T.; Hirano, M.; Hosono, H. *Nature* **2002**, *419* (6906), 462−465.

(8) Matsuishi, S.; Toda, Y.; Miyakawa, M.; Hayashi, K.; Kamiya, T.; Hirano, M.; Tanaka, I.; Hosono, H. *Science* **2003**, *301* (5633), 626−629.

(9) Boysen, H.; Kaiser-Bischoff, I.; Lerch, M.; Berendts, S.; Börger, A.; Trots, D. M.; Hoelzel, M.; Senyshyn, A. *Z. Kristallogr.* **2009**, *30* (Suppl), 323−328.

(10) Lerch, M.; Janek, J.; Becker, K. D.; Berendts, S.; Boysen, H.; Bredow, T.; Dronskowski, R.; Ebbinghaus, S. G.; Kilo, M.; Lumey, M. W.; Martin, M.; Reimann, C.; Schweda, E.; Valov, I.; Wiemhöfer, H. D. *Prog. Solid State Chem.* **2009**, *37* (2−3), 81−131.

(11) Irvine, J. T. S.; West, A. R. *Solid State Ionics* **1990**, *40/41*, 896−899.

(12) Fujita, S.; Suzuki, K.; Ohkawa, M.; Mori, T.; Iida, Y.; Miwa, Y.; Masuda, H.; Shimada, S. *Chem. Mater.* **2002**, *15* (1), 255−263.

(13) Bertoni, M. I.; Mason, T. O.; Medvedeva, J. E.; Wang, Y.; Freeman, A. J.; Poeppelmeier, K. R. *J. Appl. Phys.* **2007**, *102* (11), No. 113704.

(14) Maurelli, S.; Ruszak, M.; Witkowski, S.; Pietrzyk, P.; Chiesa, M.; Sojka, Z. *Phys. Chem. Chem. Phys.* **2010**, *12* (36), 10933−10941.

(15) Kurashige, K.; Toda, Y.; Matstuishi, S.; Hayashi, K.; Hirano, M.; Hosono, H. *Cryst. Growth Des.* **2006**, *6* (7), 1602−1605.

(16) Irvine, J. T. S.; West, A. R. *J. Appl. Electrochem.* **1989**, *19* (3), 410−412.

(17) Ebbinghaus, S. G.; Krause, H.; Syrowatka, F. *Cryst. Growth Des.* **2013**, *13* (7), 2990−2994.

(18) Ressler, T. *J. Synchrotron Radiat.* **1998**, *5*, 118−122.

(19) Shannon, R. D. *Acta Crystallogr.* **1976**, *A32*, 751−767.

(20) Rossman, G. R.; Taran, M. N. *Am. Mineral.* **2001**, *86* (7−8), 896−903.
(21) Sherman, D. M. *Phys. Chem. Minerals* **1985**, *12* (3), 161−175.
(22) Waychunas, G. A.; Rossman, G. R. *Phys. Chem. Minerals* **1983**, *9* (5), 212−215.
(23) Ebbinghaus, S.; Hu, Z.; Reller, A. *J. Solid State Chem.* **2001**, *156* (1), 194−202.
(24) Ebbinghaus, S. G. *J. Solid State Chem.* **2004**, *177* (3), 817−823.
(25) Götzfried, T.; Reller, A.; Ebbinghaus, S. G. *Inorg. Chem.* **2005**, *44* (19), 6550−6557.
(26) Ebbinghaus, S. G.; Erztoument, C.; Marozau, I. *J. Solid State Chem.* **2007**, *180*, 3393−3400.
(27) Logvinovich, D.; Aguiar, R.; Robert, R.; Trottmann, M.; Ebbinghaus, S. G.; Reller, A.; Weidenkaff, A. *J. Solid State Chem.* **2007**, *180* (10), 2649−2654.
(28) Wilke, M.; Farges, F.; Petit, P. E.; Brown, G. E.; Martin, F. *Am. Mineral.* **2001**, *86* (5−6), 714−730.